Deep-Sea Research I 55 (2008) 1364–1374

Contents lists available at ScienceDirect

Deep-Sea Research I

journal homepage: www.elsevier.com/locate/dsri

Relationship between particle size distribution and flux in the mesopelagic zone

Lionel Guidi [a,b,c,*], George A. Jackson [a], Lars Stemmann [b,c], Juan Carlos Miquel [d], Marc Picheral [b,c], Gabriel Gorsky [b,c]

[a] Department of Oceanography, Texas A&M University, College Station, TX 77843, USA
[b] Laboratoire d'Océanographie de Villefranche, Université Pierre et Marie Curie-Paris6, 06230 Villefranche-sur-Mer, France
[c] CNRS, Laboratoire d'Océanographie de Villefranche, 06230 Villefranche-sur-Mer, France
[d] Marine Environment Laboratories, International Atomic Energy Agency, 4 Quai Antoine 1er, MC98000 Monaco

ARTICLE INFO

Article history:
Received 13 July 2007
Received in revised form
15 May 2008
Accepted 27 May 2008
Available online 10 June 2008

Keywords:
Marine aggregates
Size spectrum
Sediment trap
Particle flux
POC
Settling velocity

ABSTRACT

Large aggregates commonly named "marine snow" are difficult to collect and study because of their fragile nature, but they make up the largest fraction of vertical carbon flux in the ocean. Developments in imaging sensors and computer systems have facilitated the development of *in situ* image acquisition systems that can be used to produce profiles of aggregate size distribution and abundance. However, it is difficult to collect information on the different properties of particles, such as their composition, from *in situ* images. In this paper, we relate sediment trap data to particle size (d) distributions to estimate the vertical fluxes (F) of mass, particulate organic carbon (POC), particulate inorganic carbon (PIC) and particulate organic nitrogen (PON) using simple power relationships ($F = Ad^b$). Mean aggregate fractal dimension of 2.3 and a size-dependent settling speed are determined from the flux estimations. We have used these relationships to map the distribution of mass flux along 180°W in the equatorial Pacific. Similar mass fluxes below the euphotic zone have been reported along 150°W for the same period with conventional sediment traps, supporting the accuracy of these relationships. The high spatial resolution of sedimentation processes studied *in situ* with the Underwater Video Profiler allowed us to undertake a detailed study of the role of physical processes in vertical fluxes.

1. Introduction

Large aggregates, also known as marine snow, are ubiquitous in the water column and make up a significant fraction of the particle mass and of the downward particulate organic carbon (POC) flux. More than a conveyor of the fixed carbon from the euphotic zone to depth (biological pump), large aggregates play the role of small ecosystems. They provide a unique chemical environment where both photosynthesis and microbial degradation can occur at rates greater than in the surrounding water. In addition, by moving material downward, they provide a rich food source for the mesopelagic zone.

Although important in the ocean, large aggregates are difficult to collect and study because of their fragile nature. Sediment traps have been used widely to collect settling material, to describe vertical flux and its decrease with depth, and to document the chemical transformations of settling aggregates (Turley et al., 1995; Wakeham et al., 1984, submitted). The particles collected in a sediment trap occur over a range of sizes and settling rates when suspended in the water column but lose their

* Corresponding author. Université Pierre et Marie Curie-Paris6, Laboratoire d'Océanographie de Villefranche, 06230 Villefranche-sur-Mer, France. Tel.: +33 4 93 76 38 05; fax: +33 4 93 76 38 34.
E-mail address: Lionel.Guidi@obs-vlfr.fr (L. Guidi).

0967-0637/$ - see front matter © 2008 Elsevier Ltd. All rights reserved.
doi:10.1016/j.dsr.2008.05.014

individuality in the sediment trap amalgamation. This loss of identity has been partially overcome by the use of a polyacrylamide gel in the collectors, which allows the determination of particle size distributions of these aggregates (Jannasch et al., 1980; Kiørboe et al., 1994; Waite and Nodder, 2001). Sediment traps provide an important sampling approach but do not provide the spatial coverage or the detailed descriptions of particle size distributions that are useful in mechanistic descriptions of particle dynamics.

The availability of imaging sensors and computer systems to analyze their observations has led to the development of *in situ* camera systems that can be used to produce profiles of aggregate size distribution and abundance (Asper, 1987; Davis and Pilskain, 1992; Gorsky et al., 1992; Honjo et al., 1984). Despite their ability to provide detailed particle size distributions with high spatial resolutions, imaging systems cannot describe aggregates' chemical composition without more information about the relationship between particle size and composition (Burd et al., 2007).

Particle concentrations are frequently presented as number spectra (Burd et al., 2000; Jackson, 1990; Stemmann et al., 2004b). The size spectrum of a "population" of particles is usually defined in terms of the number concentration of particles (ΔC) in a given small size range (Δs): $n = \Delta C/\Delta s$. The particle mass in that size range is $m(s)\, n(s)\, \Delta s$, and the mass flux spectrum is $m(s)\, n(s)\, w(s)\, \Delta s$, where $m(s)$ is the mass of an individual particle and $w(s)$ is its settling velocity. Any measure of particle size can be used for s, although particle diameter (d) is frequently used. The total mass flux (F) is the mass flux spectrum integrated over all particle sizes. Using diameter as a measure of particle size,

$$F = \int_0^\infty n(d)m(d)w(d)\,\mathrm{d}d \tag{1}$$

The mass of a spherical particle is given by

$$m(d) = \alpha d^3 \tag{2}$$

where $\alpha = \pi\rho/6$ and ρ is its average density. Its settling rate can be calculated using Stokes Law:

$$w(d) = \beta d^2 \tag{3}$$

where $\beta = g(\rho - \rho_0)(18\upsilon\rho_0)^{-1}$, g is gravitational acceleration, ρ_0 is the fluid density and υ is the kinematic viscosity (see Table 1 for summary of notation).

Aggregates do not have a constant density, so Eqs. (2) and (3) are not useful without more information. In fact, particle mass and settling rate are often described using relationships of the form yd^x by fitting data from observations, usually made in the surface layer (Alldredge, 1998; Alldredge and Gotschalk, 1988; Ploug and Grossart, 2000). This is equivalent to α and β being functions of d, not constant. Note that if both $w(d)$ and $m(d)$ are given by power relationships, so is the combined quantity,

$$wm = Ad^b \tag{4}$$

For the above case of constant density shown in Eqs. (1) and (2), $b = 5$.

Table 1
List of parameters and their dimension (M for mass, L for length, T for time)

Symbol	Description	Dimension
A	Constant for F_E	$\mathrm{M\,L^{-2-b}\,T^{-1}}$
a	Constant for $m(d)$ (Eq. (6))	$\mathrm{M\,L^{-D}}$
b	Constant for F_E	–
c	Constant for $w(d)$ (Eq. (7))	$\mathrm{L^{2-D}\,T^{-1}}$
d	Particle diameter	L
D	Fractal dimension	–
F	Generic flux	$\mathrm{M\,L^{-2}\,T^{-1}}$
F_E	Flux estimation using (A and b)	$\mathrm{M\,L^{-2}\,T^{-1}}$
F_T	Sediment trap flux measurement	$\mathrm{M\,L^{-2}\,T^{-1}}$
F_m, F_{poc}, F_{pic}, F_{pon}	Mass, POC, PIC and PON fluxes estimations	$\mathrm{M\,L^{-2}\,T^{-1}}$
ΔF_c	Differences between sediment trap and spectral-estimated fluxes	$\mathrm{M\,L^{-2}\,T^{-1}}$
g	Gravitational acceleration	$\mathrm{L\,T^{-2}}$
h	Coefficient to convert particle mass to particle excess of mass	–
m	Particle mass	M
n	Particle number spectrum	$\mathrm{L^{-4}}$
V	Volume of a particle	$\mathrm{L^3}$
w	Particle settling rate	$\mathrm{L\,T^{-1}}$
α	Constant for $m(d)$ (Eq. (2))	$\mathrm{M\,L^{-3}}$
β	Constant for $w(d)$ (Eq. (3))	$\mathrm{L^{-1}\,T^{-1}}$
ρ	Particle density	$\mathrm{M\,L^{-3}}$
ρ_0	Fluid density	$\mathrm{M\,L^{-3}}$
$\Delta\rho$	Particle excess density	$\mathrm{M\,L^{-3}}$
υ	Seawater viscosity	$\mathrm{L^2\,T^{-1}}$

To our knowledge, only a few studies relating aggregate size and flux have been made for the deep ocean (Asper, 1987; Ratmeyer and Wefer, 1996; Walsh and Gardner, 1992). In this paper, we relate sediment trap data to particle size distributions to estimate the vertical fluxes of mass, POC, particulate inorganic carbon (PIC) and particulate organic nitrogen (PON). This technique allows us to estimate particle fluxes with much greater horizontal and vertical resolution than is feasible with sediment traps alone. We then apply the technique to a series of profiles taken in the equatorial Pacific.

2. Material and methods

2.1. Instrument and data

We have measured particle size distributions between the surface and 1000 m depth throughout the ocean during the last 2 decades using three generations of the Underwater Video Profiler (UVP). The UVP records objects illuminated in a slab of water whose volume ranges from 0.23 to 10.50 L, depending on UVP version. An image provides information about the size and shape of particles in its field of vision which can be used to calculate particle size distributions (Gorsky et al., 1992, 2000). The detection limit has improved through time, with the minimum observed particle diameter decreasing from 250 to 90 μm; the effective maximum particle size depends on the sample volume (Table 2). The UVP is lowered on a cable

at a speed chosen to avoid overlapping regions in the images ($1\,m\,s^{-1}$). The images are recorded digitally and processed by image analysis software to yield the projected area for each particle. The equivalent spherical diameter of each particle is calculated assuming that the projected shape is a circle.

The instruments have been calibrated in a sea water tank using natural particles of different aggregate types to determine the conversion between pixel and metric unit (Stemmann et al., 2002). Different generations of instruments have been intercalibrated and the consistency of the measurements verified (Guidi et al., 2007).

We now have a database of particle size distributions from 1254 profiles for a range of seasons and locations (Fig. 1). In this study, we restricted the size range of interest to 250 μm–1.5 mm in order to use data from older UVP generations (Table 2), although we also performed the same calculations on a subset of data with the larger size range associated with UVP4a (90 μm–2 cm).

Some of the UVP profiles were made in conjunction with sediment trap deployments (Table 3). The sediment traps (model Technicap PPS5) were deployed either in moored lines (Mediterranean Sea) or drifting (Pacific and North Atlantic). Samples collected in the traps have been analyzed and total mass, organic carbon, inorganic carbon and organic nitrogen and the associated fluxes calculated.

UVP data collected within 0.2° latitude and longitude of a sediment trap location, 10 m of its depth and 5 days of its deployment were used for comparisons. An average aggregate size spectrum was calculated using the pertinent UVP data if more than one profile fit the criteria. There are 118 data sets with both particle size distributions from the UVP and sediment trap flux measurements; there are only 39 for the analysis using the larger size range.

Table 2
Definition of the size range and volume sampled characteristics of the 3 different Underwater Video Profilers (UVP) used in this study

Model	Size range	Volume sampled (L)	Reference
UVP 2a	>250 μm–1.5 mm	0.28	Gorsky et al. (1992)
UVP 2c	>150>m–1.5 mm	0.23	Gorsky et al. (1992)
UVP 3b	>90>m–5 mm	0.60	Gorsky et al. (2000)
UVP 4a	>90>m–2 cm	10.50	Gorsky et al. (2000)

2.2. Flux estimation from aggregates size

If the size distribution and the values of A and b are known, then a mass flux can be calculated from size spectra using Eqs. (1) and (4). The fluxes calculated this way can be compared to matching sediment trap observations. Because we did not know the appropriate values of A and b, we used a minimization procedure to find those two values that provided the best fit between the two fluxes—sediment trap and particle size distribution—derived.

We used the Matlab function *fminsearch* (The Mathworks, Inc., Natick, MA) to find the values of A and b that minimized the log-transformed differences (ΔF_c) between sediment trap and spectral-estimated fluxes:

$$\Delta F_c = \sum_i [\log(F_{T,i}) - \log(F_{E,i})]^2 \quad (5)$$

where $F_{T,i}$ is the sediment trap flux value and $F_{E,i}$ the associated flux based on Eq. (1) for the ith observation. The logarithmic transformation was used to give equal weight to differences for small and large fluxes. Note that

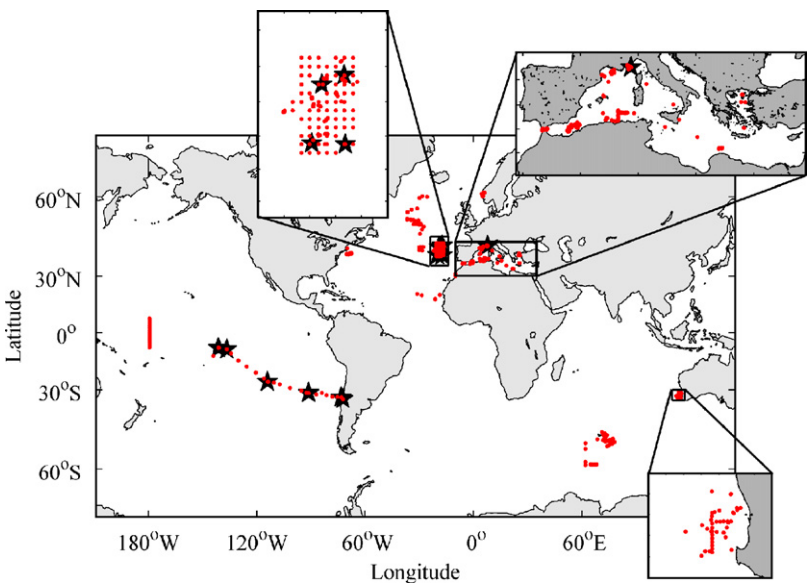

Fig. 1. Location of all Underwater Video Profiler (UVP) profiles (red dots) and associated sediment trap deployments (black stars). There were 1254 total profiles and 11 associated sediment trap locations. Details, of the sampling grid, are provided at 3 locations into the black boxes in order to make it more visible.

Table 3
Location, position and duration of the deployments of the sediments trap used in this study

Location	Station	Lat.	Long.	Begin	End	Depth	Reference
North Atlantic	NW	42.98	−19.07	2/21/01	2/6/02	400	A
North Atlantic	NW	42.98	−19.07	2/21/01	2/6/02	1000	A
North Atlantic	NE	43.83	−17.33	2/18/01	2/6/02	400	A
North Atlantic	NE	43.83	−17.33	2/18/01	2/6/02	1000	A
North Atlantic	SE	39.5	−17.25	2/18/01	2/6/02	400	A
North Atlantic	SE	39.5	−17.25	2/18/01	2/6/02	1000	A
North Atlantic	SW	39.56	−19.85	2/21/01	8/21/01	400	A
North Atlantic	SW	39.56	−19.85	2/21/01	8/21/01	1000	A
Mediterranean	Dyfamed	43.42	7.86	6/27/1987	–	100	B
Mediterranean	Dyfamed	43.42	7.86	6/27/1987	–	200	B
Mediterranean	Dyfamed	43.42	7.86	6/27/1987	–	1000	B
South Pacific	Marquise Island	−8.25	−141.14	10/26/04	10/29/04	100	C
South Pacific	Marquise Island	−8.25	−141.14	10/26/04	10/29/04	200	C
South Pacific	HNLC	−9	−136.53	10/31/04	11/2/04	100	C
South Pacific	HNLC	−9	−136.53	10/31/04	11/2/04	200	C
South Pacific	Central Gyre	−26.04	−114.02	11/12/04	11/16/04	200	C
South Pacific	Central Gyre	−26.04	−114.02	11/12/04	11/16/04	400	C
South Pacific	East Gyre	−31.52	−91.25	11/25/04	11/30/04	200	C
South Pacific	East Gyre	−31.52	−91.25	11/25/04	11/30/04	300	C
South Pacific	Chilean upwelling	−33.58	−73.23	12/6/04	12/8/04	100	C
South Pacific	Chilean upwelling	−33.58	−73.23	12/6/04	12/8/04	200	C
South Pacific	Chilean upwelling	−34.36	−72.26	12/9/04	12/11/04	100	C
South Pacific	Chilean upwelling	−34.36	−72.26	12/9/04	12/11/04	200	C

References: A—Guieu et al., 2005; B—Stemmann et al., 2002; C—Miquel et al., 2006.

the sample integration is only for particles between 250 μm and 1.5 mm, not the 0–∞ shown in Eq. (1).

We also tested the ability of a previously determined set of relationships for w and m to match the ways of estimating fluxes. Alldredge and Gotschalk (1988) calculated that their diatom aggregates in the surface waters off Santa Barbara, CA, followed the relationships $m = 8.8d^{1.125}$ and $w = 50d^{0.26}$ (in mg m^{-3} and m d^{-1}), implying that A equals 440 (in mg m^{-2} mm^{-b} d^{-1}) and b equals 1.385.

2.3. Error estimation of the parameters

The minimization procedure yields only one pair of parameter values. We used a jackknife procedure to estimate the errors of the estimates. The minimization was performed on 1000 subsamples one third the size of the original data set and composed of data pairs selected randomly from the original data set. The results provide us with the frequency distribution of A and b.

3. Results

3.1. Comparing size spectral flux estimates to observed fluxes

Pearson's correlation coefficient between the two fluxes is 0.40 when Alldredge and Gotschalk (1988) values for A and b are used. However, the particle size estimate of flux consistently overestimates the sediment trap fluxes, with 95% of the estimates larger than the observations (Fig. 2). Furthermore, the overestimation can reach a factor of 100.

The minimization procedure provided flux estimates that are better for mass (F_m), POC (F_{poc}), PIC (F_{pic}) and PON (F_{pon}) fluxes (Fig. 3). Pearson's correlation coefficients between the two fluxes vary from 0.57 to 0.73 for F_{pic} and F_{pon}, respectively. The values of b are quite consistent for the different fluxes, with largest differences equal to 0.4 between F_m and F_{pon} (3.52 and 3.93). The standard deviations on the values for b estimated using the jackknife procedure are 0.7–0.8 (Table 4). Most of the differences in the parameter values for the different material fluxes are for A and reflect the material composition. The ratio F_m to F_{poc} is about 10 and F_{poc} to F_{pon} is 6.2, similar to the Redfield ratio for C:N of 6.6 and reflecting the sediment trap data.

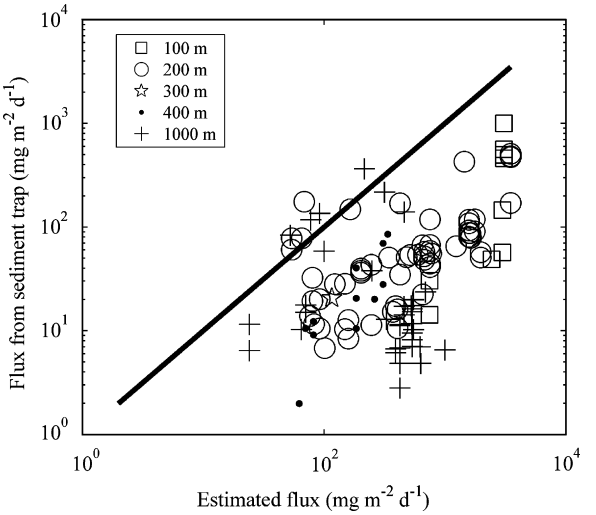

Fig. 2. Comparison of measured sediment trap mass flux with that calculated using size spectra and Alldredge and Gotschalk (1988) relationships ($n = 118$). Symbols represent trap deployment depths.

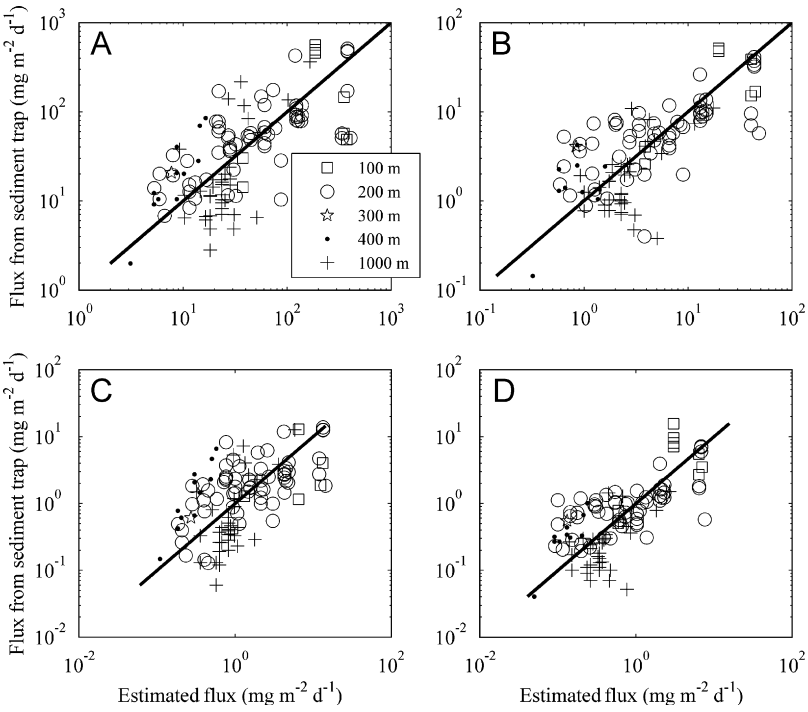

Fig. 3. Measured mass (A), particulate organic carbon (POC; B), particulate inorganic carbon (PIC; C) and particulate organic nitrogen (PON; D) fluxes by sediment traps, compared to the estimation of the mass, POC, PIC and PON fluxes using the UVP and the relationships between aggregate size and fluxes from this study (cf. Eqs. (3)–(6), $n = 118$. Symbols represent trap deployment depths.

Table 4
Coefficient (A) and exponent (b) and their associated standard deviation (STD) of the empirical relationship between the aggregate size and the related mass, particulate organic carbon (POC), particulate inorganic carbon (PIC) and particulate organic nitrogen (PON) fluxes determined by minimization of the flux estimations by the Underwater Video Profiler (UVP) and the sediment trap measurements, $n = 118$

Fluxes	Symbol	A	STD A	b	STD b	R^2	P
Generic relationship: $F = Ad^b$							
Mass	F_m	109.5	32.6	3.52	0.72	0.70	<0.0001
POC	F_{poc}	12.5	3.40	3.81	0.70	0.73	<0.0001
PIC	F_{pic}	3.97	1.13	3.60	0.76	0.57	<0.0001
PON	F_{pon}	2.02	0.59	3.93	0.82	0.71	<0.0001

There appears to be little systematic statistical difference in the relationship between estimated and observed fluxes within the depth range of 100 and 1000 m. Even if there is little difference with depth, mass and PIC have similar evolution, as well as POC and PON fluxes (Fig. 4). The mass flux is highly variable and ranges from 10 to 1000 mg m^{-2} d^{-1}.

3.2. Error estimation

The standard deviations of A and b from the jackknife procedure are ~30% and ~20% of the minimization values for all of the different fluxes (F_m, F_{poc}, F_{pic} and F_{pon}; Table 4).

A map of ΔF for a range of parameter values provides a different perspective on the sensitivity of the residual to these parameters (Fig. 5). The results show a well-defined region for the minimum. The values of A and b calculated for the 1000 subsamples in the jackknife procedure fall in the minimum region. They follow a normal distribution (Kolmogorov–Smirnov test significant at the 5% level) from which the mean and the standard deviation have been calculated (Table 4). Results for the other relationships (F_{poc}, F_{pic} and F_{pon}) are similar but not shown.

4. Discussion

The flux measurements cover three orders of magnitude, a range that can hide variations that are absolutely small but locally significant. Such variation is consistent with fluxes measured in oligotrophic and eutrophic regions (Fig. 3A). Despite the variability of the several flux measures, simple power relationships relate them to the particle size spectra. This has several implications.

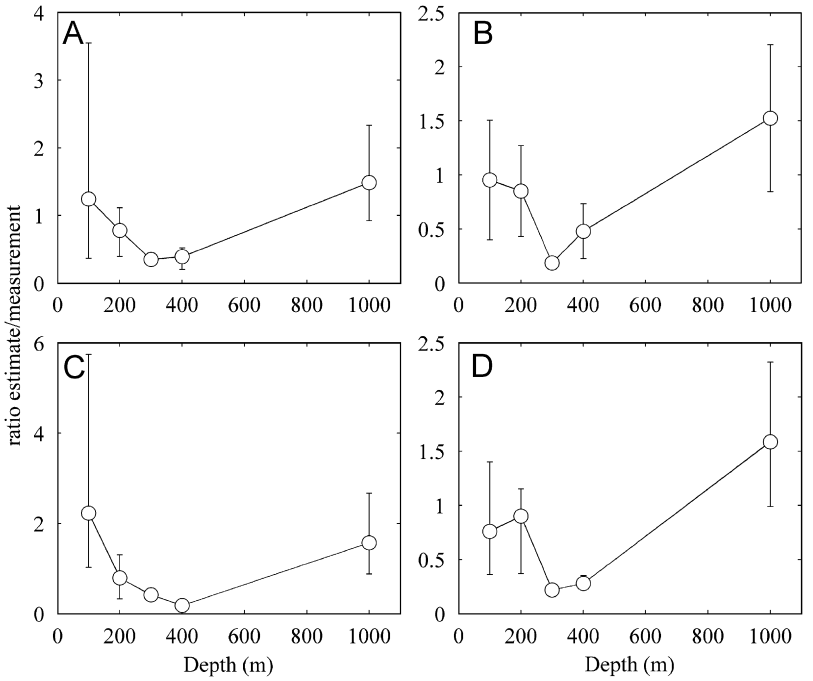

Fig. 4. Median, first and third quartiles of ratio between estimates and measurements of the (A) mass fluxes, (B) POC fluxes, (C) PIC fluxes and (D) PON fluxes as a function of the depth of sediment traps.

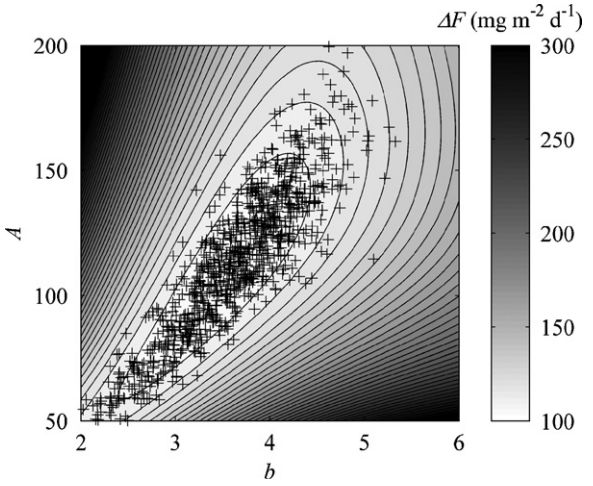

Fig. 5. Residual error ΔF as a function of values of A, b for the mass flux F_m. The best fit values were $A = 109.5$ and $b = 3.52$. Darker regions represent greater values for ΔF in mg m^{-2} d^{-1}. The crosses correspond to the values calculated during the jackknife error analysis. They are all located in the area where the residues are the smallest.

4.1. Estimation of the fractal dimension of the aggregates

The relationships of fractal geometry have been used to estimate fractal dimensions (D) (Logan and Wilkinson, 1990) from velocity measurements and velocity measurements from fractal dimensions (Jackson et al., 1997). If the particle size is given by particle diameter (d), then its mass is

$$m(d) = ad^D \tag{6}$$

The sinking rate (w) of the same aggregate, derived from Eqs. (3) and (6), is

$$w(d) = cd^{D-1} \tag{7}$$

where $c = gah/3\pi\upsilon\rho_0$ and h is the ratio of particle excess mass to particle mass. Hence, $wm = acd^{2D-1}$ and $D = (b+1)/2$. It follows that the flux of particles within a size range of d to $d+\Delta d$ is

$$\Delta F(d) = nAd^{2D-1}\,\Delta d \tag{8}$$

where $A = ac$.

The mean fractal dimensions corresponding to our results range from 2.26 to 2.46. Fractal dimensions of marine aggregates have been estimated to be between 1.3 and 3.75 (Jackson et al., 1997; Jiang and Logan, 1991; Li and Logan, 1995). Values of $D > 3$ can arise from measurement errors or use of an inappropriate model when observations are analyzed. The aggregate fractal dimension derived from F_m is high compared to the values of 1.125–1.3 reported by Alldredge (1998) for visible aggregates in a rich diatom upwelling system off California. Our study is focused on deeper aggregates (100–1000 m depth). Aggregates below the surface mixed layer have been altered as they fall, which may account for the higher values than those of Alldredge. An increase in fractal dimension with depth implies a decrease in porosity. Different mechanisms can lead to such results. The physical action of the fluid going through the aggregate as it sinks may compact them and decrease their porosity (Logan and Kilps, 1995). There are a variety of processes that consume and redistribute matter in settling aggregates, including physical coagulation

(Jackson, 1990), microbial degradation (Kiørboe, 2001; Ploug and Grossart, 2000), zooplankton feeding (Graham et al., 2000; Jackson and Kiørboe, 2004; Stemmann et al., 2004a) and zooplankton fragmentation (Goldthwait et al., 2004). Biological processes mentioned previously lead to a preferential removal of organic carbon relative to inorganic carbon. These happen at different rates spatially and temporally but appear to transform the aggregate properties in a consistent way everywhere on the globe. For example, they may act to decrease the median size of the aggregate and therefore decrease the related flux. Despite the range of systems that we used, we cannot rule out the possibility that there are regional differences which we have not seen. Further investigations need to be done in order to see what mechanisms impact the porosity of the aggregates and how this porosity can change with depth.

The chemical composition and packing of the aggregates determines their mass and settling rates as a function of diameter. We expect aggregates having the same components to result in a unique size to settling rate and mass flux relationship. Only small changes have been observed between 100 and 1000 m (Fig. 4) that could be caused by change in trap collection efficiencies in the 100–400 m samples. However, the mass, POC and PON ratios change with depth (Boyd et al., 1999), suggesting that most of the aggregate transformation occurs in the first 100 m of the water column as previously shown by sediment trap data (Berelson, 2001; Karl et al., 1988; Martin et al., 1987).

4.2. The size measurement issue

The relationships described here are based on the UVP aggregate size measurements. Many different instruments have been used these last 20 years to describe the abundance and the size distribution of aggregates. Instruments as different as the Coulter Counter (Beckman Coulter, Inc, Fullerton, CA) and the UVP measure different particle properties. The Coulter Counter measures the change in electrical resistance as a particle passes through a small orifice which is usually assumed to be proportional to the conserved particle volume (Jackson et al., 1995; Li and Logan, 1995; McCave, 1983). Optical imaging techniques such as the UVP determine a particle's size by measuring its projected area on a two-dimensional plane. This area corresponds to the number of pixels that cover the image converted in metric units (Guidi et al., 2007; MacIntyre et al., 1995; Stemmann et al., 2002). These two examples represent a small fraction of the techniques available to obtain the size distribution of particles in the oceanic environment. Therefore, the fact that relationships described in this article can be used with different instruments is not obvious before a careful analysis of the instrument properties has been done.

Multi-instrumental comparison studies are actually available. The size spectrum and the fractal dimension of aggregates provide powerful tools to compare results from these different instruments (Jackson et al., 1995, 1997). The authors found that the size spectrum calculated by different instruments can be compared after all measurements have been transformed to an optical diameter basis. The relationships used here could then be applied to any kind of instrument assuming that the conversion coefficients between instruments are correctly estimated.

4.3. Estimation of the settling speed of the aggregates

The settling speed is a function of aggregate diameter and fractal dimension:

$$w(d) = \frac{hagd^{D-1}}{3\pi\rho_0\upsilon} \tag{9}$$

where $a = \sqrt{A3\pi\rho_0\upsilon/hg}$ (derived from Eqs. (4), (6) and (7)).

The use of Eq. (9) leads to settling rates of 1.8, 32 and 248 m d^{-1} for particles of 100 μm, 1 mm and 5 mm (Fig. 6A). These estimates are in the range of reported settling rates (Syvitski et al., 1995; Peterson et al., 2005; Lee et al., submitted).

The distribution of mass flux depends on the particle size distribution as well as the mass and settling relationships. Observations on the relative timing of sedimentation events through the water column have yielded estimates that material typically settles at 100–400 m d^{-1} (Berelson, 2002; Fowler and Knauer, 1986; Shanks, 2002). More recent measurements of settling velocity at the French Dyfamed site yield a median velocity for the flux of about 150 m d^{-1} with a significant fraction of particles settling at 200–500 m d^{-1} (Peterson et al., 2005). Using a representative size spectrum determined using the UVP and our relationship for *wm* (Eq. (4)) as a function of *d*, we calculate a mean settling rate of 115 m d^{-1}, corresponding to the fall velocity of a 2.7 mm aggregate (Fig. 6B and C). The flux was dominated by the large aggregates between 400 μm and 4 mm (Fig. 6A). For the same size spectrum but with the Alldredge and Gotschalk (1988) relationship, the mean settling rate is 35 m d^{-1}, corresponding to a median aggregate size of 250 μm. This flux would be dominated by aggregates smaller than 400 μm.

4.4. Using a larger size range

While the size range that we used for the size spectra covers a large range of settling particles, it does not cover all particles. We made the previous parameter estimation using spectra covering the limited 250 μm–1.5 mm size range. When we applied our technique to UVP4a size spectra profiles with the expanded 100 μm to 2 cm size range ($n = 200$), the calculated fluxes averaged 2.3 times those calculated for the smaller range. Most of this increase was associated with the inclusion of larger particles. There were uncertainties in the original parameter values of 20–30%. The flux values calculated with the larger size range are comparable to the uncertainties in fluxes associated with the parameter ranges and the smaller particle size range. Interestingly, when we used

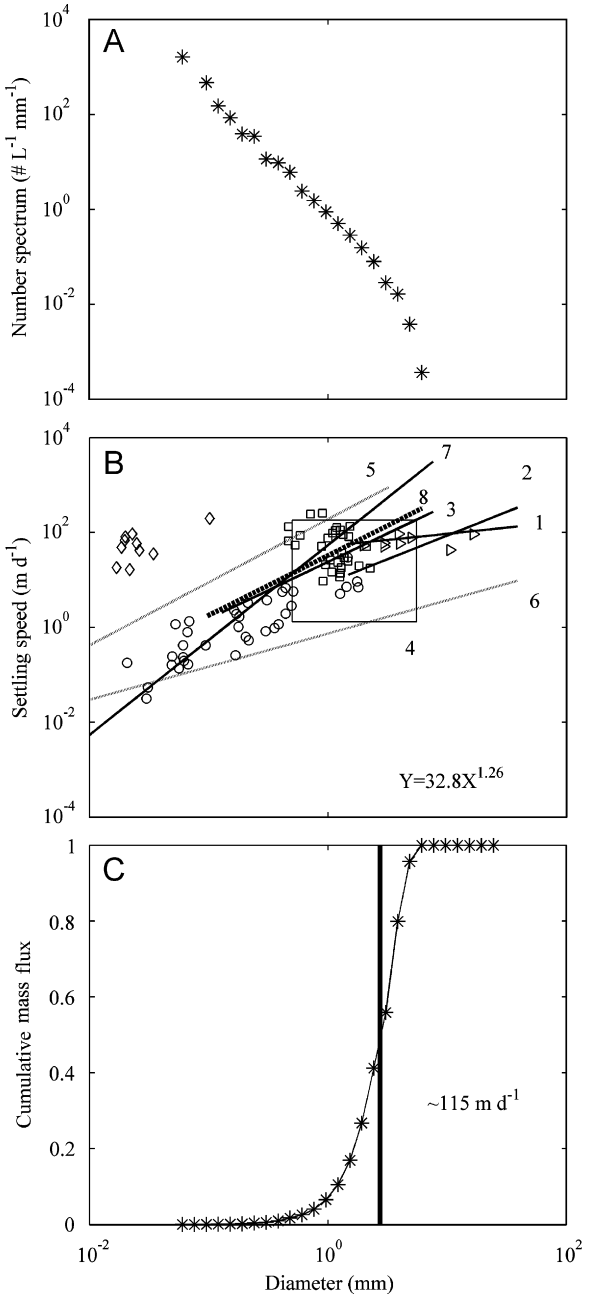

Fig. 6. Aggregate settling velocity and mass flux based on size distribution. (A) Typical number spectrum from the UVP database profiles. (B) Particle settling velocity as a function of particle diameter measured by different authors (from Stemmann et al., 2004b; Circle: Smayda, 1970; triangle: Shanks and Trent, 1980; diamond: Carder et al., 1982; square: Azetsu-Scott and Johnson, 1992; Empirical relationships: 1—Alldredge and Gotschalk, 1988; 2—Alldredge and Gotschalk, 1989; 3—Syvitski et al., 1995; 4—Diercks and Asper, 1997). Settling velocities calculated using the coagulation model (Stemmann et al., 2004b) with different parameter values (5—$\Delta\rho = 0.08$, $D = 2.33$; 6—$\Delta\rho = 0.01$, $D = 1.79$) are also reported. The regression line 7 is the settling speed predicted by Stokes Law. The dashed line 8 is the settling speed calculated in this paper. (C) Normalized cumulative flux calculated on the number spectrum (a) with the mass flux relationship (Eq. (8)); the black line represents 50% value of the mass flux.

the Alldredge and Gotschalk (1988) relationship, the flux was greater by a similar proportion, but most of the increase came from the greater number of small particles. While it is clear that the parameters from m and w would change if the minimization procedure were performed with a greater particle size range, the change is small compared to the large range of fluxes observed and the parameter uncertainties.

4.5. Application

We have used these results to map the vertical distribution of mass flux along a transect across the equator at 180°W between 100 and 1000 m using data from the Ebene cruise (Gorsky et al., 2003). Similar mass fluxes below the euphotic zone (200 m) have been reported for a transect along 150°W for the same period with conventional sediment traps, bolstering the accuracy of these relationships (Fig. 7). However, there are three processes that can highly impact trap measurements. The trap collection efficiency depends on how a trap interacts with the water flowing around it and collects aggregates in a hydrodynamic environment. Swimmers are another source of sample "contamination". The third perturbation corresponds to the possible resolubilization or remineralization of aggregate caught in the traps (Buesseler et al., 2007). These biases have to be kept in mind when sediment trap data are compared to flux estimation from aggregate size distribution. In our case the strong equatorial undercurrent may change trapping collection efficiency. However, data were used to compare fluxes order of magnitude and variation and not absolute values.

The higher vertical and spatial resolution of the flux provides more information on its spatial variability and therefore, on the processes at the origin of the export than deployed sediment traps. The South Equatorial Current (SEC) was flowing westward at 180°, between 5°S and 4°N, and the North Equatorial Countercurrent (NECC) flowed eastward, north of 4°N. The South Equatorial Counter Current (SECC) was 6°S (Eldin and Rodier, 2003). Subsurface flow consisted of the eastward flowing Equatorial Under-Current (EUC), centered at the equator below 100 m. The South and North Subsurface Countercurrents (SSCC, NSCC) also flowed eastward below 200 m south of 6°S and north of 2°N, respectively (Fig. 8). The total concentration of chlorophyll a (Tchl a) was highest between the equator and 5°N, averaging 0.21 $\mu g\,L^{-1}$ and not exceeding 0.36 $\mu g\,L^{-1}$. Tchl a maxima were localized in the 60–100-m depth strata at the equator, 4–6°S and 5–6°N (Brown et al., 2003). These strong features create physical gradients probably at the origin of localized higher downward export (6°S and 5°N) of the surface production (Walsh et al., 1997). Areas with high mass fluxes were localized immediately below the SEC, NECC and SECC with fluxes 3–5 times higher than in the surrounding water. Similar flux heterogeneity had been observed in the North Atlantic where mesoscale eddies were recorded (Guidi et al., 2007). Large mass flux is located between 400 and 700 m depth at the equator. Increases in particle flux with depth have been attributed to horizontal advection from boundaries (Gardner and

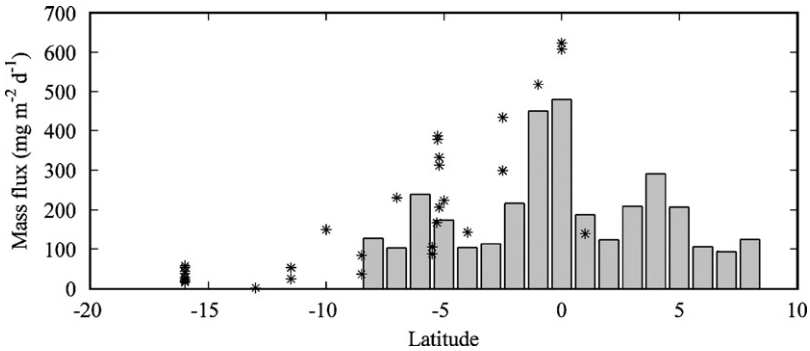

Fig. 7. Sediment trap mass flux below the euphotic zone (200 m) in mg m^{-2} d^{-1} along 150°W (black asterisk) redrawn from Raimbault et al. (1999) compared to estimated mass flux from aggregates size distribution along 180°W (gray bars) at the same depth.

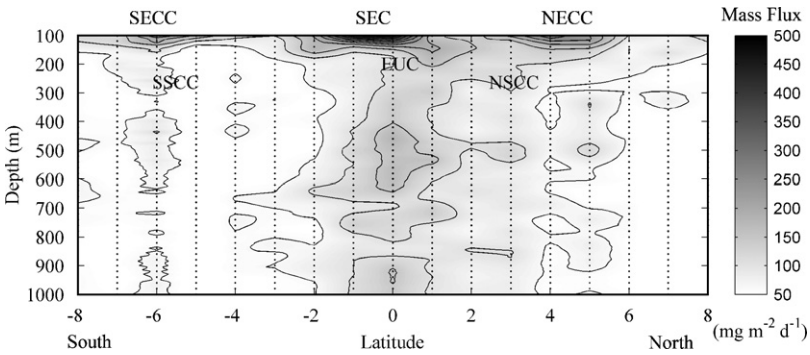

Fig. 8. Estimation of the mass flux for a north–south transect at 180°W in the equatorial Pacific Ocean, based on the size aggregate distribution. $A = 109.5$ and $b = 3.52$ for the size to mass flux relationship (Table 3) in a dynamic ocean context: SECC and NECC (South and North Equatorial Counter Current), SSCC and NSCC (South and North Subsurface Counter Current), SEC (South Equatorial Current) and EUC (Equatorial Under-Current). The dots correspond to the sampling grid.

Richardson, 1992), vertical migration and midwater biological activities (Karl et al., 1996). According to the physical field, this flux increase could be the result of an accumulation of the aggregates slipping along the borders of the EUC (Gorsky et al., 2003). Unfortunately, the lack of biological mesopelagic data at this location precludes a clear conclusion.

5. Conclusion

The data presented in this article allowed a comparison between flux measurements made with sediment traps and instantaneous flux estimated by an imaging system. We have shown that the size distribution of aggregates can be related to the mass, POC, PIC and PON flux measurements in the mesopelagic zone. In the future, similar procedures using aggregate size distribution, sediment trap flux measurements and thorium/uranium profiles will probably increase the accuracy of the flux estimations.

It has been shown recently that the vertical distribution of aggregates and the resulting carbon flux in the mesopelagic zone can be driven by the mesoscale circulation (Guidi et al., 2007; Stemmann et al., 2008). Thus, in an eddy area, only a high spatial and temporal mapping of the flux can lead to a better understanding of the process that regulates the carbon flux in a dynamic ocean. The development of indirect estimates of particle flux allowed by our relationships will increase our ability to ameliorate both vertical and horizontal resolution of particle fluxes in the deep ocean.

Acknowledgments

This research was undertaken in the framework of the MBP-Front and DYFAMED CNRS-INSU French JGOFS programs. We thank the officers and crews of R.V. *L'Atalante*, *Thalassa*, *Korotneff* and *Tethys II* for their valuable assistance and support. We also thank the different operators of the Underwater Video Profiler. The manuscript was improved with valuable comments from three anonymous reviewers. This research was funded by the PROOF project by CNRS/INSU and the ZOOPNEC program, part of the French framework of the PNEC project. This work was supported by NSF Grants OCE-0352127 and OCE-0327644. L. Guidi was financially supported by Ministère de la l'Education et de la Recherche and CNRS (France). The International Atomic Energy Agency is grateful for the support provided to its

Marine Environment Laboratories by the Government of the Principality of Monaco.

References

Alldredge, A., 1998. The carbon, nitrogen and mass content of marine snow as a function of aggregate size. Deep-Sea Research I 45 (4–5), 529–541.

Alldredge, A.L., Gotschalk, C., 1988. In situ settling behavior of marine snow. Limnology and Oceanography 33 (3), 339–351.

Alldredge, A.L., Gotschalk, C.C., 1989. Direct observations of the mass flocculation of diatom blooms: characteristics, settling velocities and formation of diatom aggregates. Deep-Sea Research 36 (2A), 159–171.

Asper, V.L., 1987. Measuring the flux and sinking speed of marine snow aggregates. Deep-Sea Research I 34 (1), 1–17.

Azetsu-Scott, K., Johnson, B.D., 1992. Measuring physical characteristics of particles: a new method of simultaneous measurement for size, settling velocity and density of constituent matter. Deep-Sea Research I 39 (6), 1057–1066.

Berelson, W.M., 2001. The flux of particulate organic carbon into the ocean interior: a comparison of four US JGOFS regional studies. Oceanography 14, 59–67.

Berelson, W.M., 2002. Particle settling rates increase with depth in the ocean. Deep-Sea Research II 49 (1–3), 237–251.

Boyd, P.W., Sherry, N.D., Berges, J.A., Bishop, J.K.B., Calvert, S.E., Charette, M.A., Giovannoni, S.J., Goldblatt, R., Harrison, P.J., Moran, S.B., Roy, S., Soon, M., Strom, S., 1999. Transformations of biogenic particulates from the pelagic to the deep ocean realm. Deep-Sea Research II 46 (11–12), 2761–2792.

Brown, S.L., Landry, M.R., Neveux, J., Dupouy, C., 2003. Microbial community abundance and biomass along a 180 degrees transect in the equatorial Pacific during an El Nino-Southern Oscillation cold phase. Journal of Geophysical Research. C. Oceans 108 (C12).

Buesseler, K.O., Antia, A.N., Chen, M., Fowler, S.W., Gardner, W.D., Gustafsson, O., Harada, K., Michaels, A.F., van der Loeff, M.R., Sarin, M., Steinberg, D.K., Trull, T., 2007. An assessment of the use of sediment traps for estimating upper ocean particle fluxes. Journal of Marine Research 65 (3), 345–416.

Burd, A.B., Moran, S.B., Jackson, G.A., 2000. A coupled adsorption–aggregation model of the POC/Th-234 ratio of marine particles. Deep-Sea Research I 47 (1), 103–120.

Burd, A.B., Jackson, G.A., Moran, S.B., 2007. The role of the particle size spectrum in estimating POC fluxes from 234Th/238U disequilibrium. Deep-Sea Research I 54 (6), 897–918.

Carder, K.L., Steward, R.G., Betzer, P.R., 1982. In situ holographic measurements of the sizes and settling rates of oceanic particulates. Journal of Geophysical Research 87 (C8), 5681–5685.

Davis, D.L., Pilskain, C.H., 1992. Measurements with underwater video-camera field width calibration and structured lighting. Marine Technology Society Journal 26 (4), 13–19.

Diercks, A.R., Asper, V.L., 1997. In situ settling speeds of marine snow aggregates below the mixed layer: Black Sea and Gulf of Mexico. Deep-Sea Research I 44 (3), 385–398.

Eldin, G., Rodier, M., 2003. Ocean physics and nutrient fields along 180 degrees during an El Nino-Southern Oscillation cold phase. Journal of Geophysical Research. C. Oceans 108 (C12).

Fowler, S.W., Knauer, G.A., 1986. Role of large particles in the transport of elements and organic compounds through the oceanic water column. Progress in Oceanography 16 (3), 147–194.

Gardner, W.D., Richardson, M.J., 1992. Particle export and resuspension fluxes in the western North Altantic. In: Rowe, G.T., Pariente, V. (Eds.), Deep-Sea Food Chains and the Global Carbon Cycle. Kluwer Academic publishers, Netherlands, pp. 339–364.

Goldthwait, S., Yen, J., Brown, J., Alldredge, A., 2004. Quantification of marine snow fragmentation by swimming euphausiids. Limnology and Oceanography 49 (4), 940–952.

Gorsky, G., Aldorf, C., Kage, M., Picheral, M., Garcia, Y., Favole, J., 1992. Vertical distribution of suspended aggregates determined by a new underwater video profiler. In: Nival, P., Boucher, J., Bhaud, M. (Eds.), 3ème Colloque du Programme National sur le Determinisme du Recrutement, Nantes (France), 1–3 October 1991. Annales de l'Institut oceanographique, Paris, Nantes (France), pp. 275–280.

Gorsky, G., Picheral, M., Stemmann, L., 2000. Use of the Underwater Video Profiler for the study of aggregate dynamics in the North Mediterranean. Estuarine Coastal and Shelf Science 50 (1), 121–128.

Gorsky, G., le Borgne, R., Picheral, M., Stemmann, L., 2003. Marine snow latitudinal distribution in the equatorial Pacific along 180 degree. Journal of Geophysical Research. C. Oceans 108 (C12).

Graham, W.M., MacIntyre, S., Alldredge, A.L., 2000. Diel variations of marine snow concentration in surface waters and implications for particle flux in the sea. Deep-Sea Research I 47 (3), 367–395.

Guidi, L., Stemmann, L., Legendre, L., Picheral, M., Prieur, L., Gorsky, G., 2007. Vertical distribution of aggregates (>110 μm) and mesoscale activity in the northeastern Atlantic: effects on the deep vertical export of surface carbon. Limnology and Oceanography 52 (1), 7–18.

Guieu, C., Roy-Barman, M., Leblond, N., Jeandel, C., Souhaut, M., Le Cann, B., Dufour, A., Bournot, C., 2005. Vertical particle flux in the northeast Atlantic Ocean (POMME experiment). Journal of Geophysical Research. C. Oceans 110 (C7).

Honjo, S., Doherty, K.W., Agrawal, Y.C., Asper, V.L., 1984. Direct optical assessment of large amorphous aggregates (marine snow) in the deep ocean. Deep-Sea Research I 31 (1), 67–76.

Jackson, G.A., 1990. A model of the formation of marine algal flocs by physical coagulation processes. Deep-Sea Research 37 (8A), 1197–1211.

Jackson, G.A., Kiørboe, T., 2004. Zooplankton use of chemodetection to find and eat particles. Marine Ecology-Progress Series 269, 153–162.

Jackson, G.A., Logan, B.E., Alldredge, A.L., Dam, H.G., 1995. Combining particle-size spectra from a mesocosm experiment measured using photographic and aperture impedance (Coulter and Elzone) techniques. Deep-Sea Research II 42 (1), 139–157.

Jackson, G.A., Maffione, R., Costello, D.K., Alldredge, A.L., Logan, B.E., Dam, H.G., 1997. Particle size spectra between 1 μm and 1 cm at Monterey Bay determined using multiple instruments. Deep-Sea Research I 44 (11), 1739–1767.

Jannasch, H.W., Zafiriou, O.C., Farrington, J.W., 1980. A sequencing sediment trap for time-series studies of fragile particles. Limnology and Oceanography 25 (5), 939–943.

Jiang, Q., Logan, B.E., 1991. Fractal dimensions of aggregates determined from steady-state size distributions. Environmental Science & Technology 25 (12), 2031–2038.

Karl, D.M., Knauer, G.A., Martin, J.H., 1988. Downward flux of particulate organic-matter in the ocean—a particle decomposition paradox. Nature 332 (6163), 438–441.

Karl, D.M., Christian, J.R., Dore, J.E., Hebel, D.V., Letelier, R.M., Tupas, L.M., Winn, C.D., 1996. Seasonal and interannual variability in primary production and particle flux at Station ALOHA. Deep-Sea Research II 43 (2–3), 539–568.

Kiørboe, T., 2001. Formation and fate of marine snow: small-scale processes with large-scale implications. Scientia Marina 65, 57–71.

Kiørboe, T., Lundsgaard, C., Olesen, M., Hansen, J.L.S., 1994. Aggregation and sedimentation processes during a spring phytoplankton bloom—a field experiment to test coagulation theory. Journal of Marine Research 52 (2), 297–323.

Lee, C., Peterson, M.L., Wakeham, S.G., Armstrong, R.A., Cochran, J.K., Miquel, J.C., Fowler, S., Hirschberg, D., Beck, A., Xue, J., accepted. Particulate organic matter and ballast fluxes measured using time-series and settling velocity sediment traps in the northwestern Mediterranean Sea. Deep-Sea Research II.

Li, X.Y., Logan, B.E., 1995. Size distributions and fractal properties of particles during a simulated phytoplankton bloom in a mesocosm. Deep-Sea Research II 42 (1), 125–138.

Logan, B.E., Kilps, J.R., 1995. Fractal dimensions of aggregates formed in different fluid mechanical environments. Water Research 29 (2), 443–453.

Logan, B.E., Wilkinson, D.B., 1990. Fractal geometry of marine snow and other biological aggregates. Limnology and Oceanography 35 (1), 130–136.

MacIntyre, S., Alldredge, A.L., Gotschalk, C.C., 1995. Accumulation of marine snow at density discontinuities in the water column. Limnology and Oceanography 40 (3), 449–468.

Martin, J.H., Knauer, G.A., Karl, D.M., Broenkow, W.W., 1987. VERTEX: carbon cycling in the Northeast Pacific. Deep-Sea Research 34 (2A), 267–285.

McCave, I.N., 1983. Particulate size spectra, behavior, and origin of nepheloid layers over the Nova Scotian continental rise. Journal of Geophysical Research. C. Oceans 88 (C12), 7647–7666.

Miquel, J.C., Gasser, B., Claustre, H., 2006. Export Fluxes in Contrasting Environments of the South-East Pacific Ocean Derived From Drifting Sediment traps (BIOSOPE). Eos Trans. AGU. 87(52), Fall Meet. Suppl., OS13C-1569.

Peterson, M.L., Wakeham, S.G., Lee, C., Askea, M.A., Miquel, J.C., 2005. Novel techniques for collection of sinking particles in the ocean and determining their settling rates. Limnology and Oceanography—Methods 3, 520–532.

Ploug, H., Grossart, H.P., 2000. Bacterial growth and grazing on diatom aggregates: respiratory carbon turnover as a function of aggregate size and sinking velocity. Limnology and Oceanography 45 (7), 1467–1475.

Raimbault, P., Slawyk, G., Boudjellal, B., Coatanoan, C., Conan, P., Coste, B., Garcia, N., Moutin, T., Pujo-Pay, M., 1999. Carbon and nitrogen uptake and export in the equatorial Pacific at 150 degrees W: evidence of an efficient regenerated production cycle. Journal of Geophysical Research. C. Oceans 104 (C2), 3341–3356.

Ratmeyer, V., Wefer, G., 1996. A high resolution camera system (ParCa) for imaging particles in the ocean: system design and results from profiles and a three-month deployment. Journal of Marine Research 54 (3), 589–603.

Shanks, A.L., 2002. The abundance, vertical flux, and still-water and apparent sinking rates of marine snow in a shallow coastal water column. Continental Shelf Research 22 (14), 2045–2064.

Shanks, A.L., Trent, J.D., 1980. Marine snow-sinking rates and potential role in vertical flux. Deep-Sea Research I 27 (2), 137–143.

Smayda, T.J., 1970. The suspension and sinking of phytoplankton in the sea (RV). Oceanography and Marine Biology 8, 353–414.

Stemmann, L., Gorsky, G., Marty, J.C., Picheral, M., Miquel, J.C., 2002. Four-year study of large-particle vertical distribution (0–1000 m) in the NW Mediterranean in relation to hydrology, phytoplankton, and vertical flux. Deep-Sea Research II 49 (11), 2143–2162.

Stemmann, L., Jackson, G.A., Gorsky, G., 2004a. A vertical model of particle size distributions and fluxes in the midwater column that includes biological and physical processes—Part II: application to a three year survey in the NW Mediterranean Sea. Deep-Sea Research I 51 (7), 885–908.

Stemmann, L., Jackson, G.A., Ianson, D., 2004b. A vertical model of particle size distributions and fluxes in the midwater column that includes biological and physical processes—Part I: model formulation. Deep-Sea Research I 51 (7), 865–884.

Stemmann, L., Prieur, L., Legendre, L., Taupier-Letage, I., Picheral, M., Guidi, L., Gorsky, G., 2008. Effects of frontal processes on marine aggregate dynamics and fluxes: an interannual study in a permanent geostrophic front (NW Mediterranean). Journal of Marine Systems 70 (1–2), 1–20.

Syvitski, J.P.M., Asprey, K.W., Leblanc, K.W.G., 1995. In-situ characteristics of particles settling within a deep-water estuary. Deep-Sea Research II 42 (1), 223–256.

Turley, C.M., Lochte, K., Lampitt, R.S., 1995. Transformations of biogenic particles during sedimentation in the northeastern Atlantic. Philosophical Transactions of the Royal Society of London Series B—Biological Sciences 348 (1324), 179–189.

Waite, A.M., Nodder, S.D., 2001. The effect of in situ iron addition on the sinking rates and export flux of Southern Ocean diatoms. Deep-Sea Research II 48 (11–12), 2635–2654.

Wakeham, S.G., Lee, C., Farrington, J.W., Gagosian, R.B., 1984. Biogeochemistry of particulate organic-matter in the oceans—results from sediment trap experiments. Deep-Sea Research I 31 (5), 509–528.

Wakeham, S.G., Lee, C., Peterson, M.L., Liu, Z., Szlosek, J., Putnam, I., Xue, J., accepted. Organic compound composition and fluxes in the Twilight Zone-time series and settling velocity sediment traps during MEDFLUX. Deep-Sea Research II.

Walsh, I.D., Gardner, W.D., 1992. A comparison of aggregate profiles with sediment trap fluxes. Deep-Sea Research 39 (11A–12A), 1817–1834.

Walsh, I.D., Gardner, W.D., Richardson, M.J., Chung, S.P., Plattner, C.A., Asper, V.L., 1997. Particle dynamics as controlled by the flow field of the eastern equatorial Pacific. Deep-Sea Research II 44 (9–10), 2025–2047.